Soliton structure in crystalline acetanilide

J. C. Eilbeck,* P. S. Lomdahl, and A. C. Scott
Center for Nonlinear Studies, Los Alamos National Laboratory, Los Alamos, New Mexico 87545
(Received 2 April 1984)

The theory of self-trapping of amide I vibrational energy in crystalline acetanilide is studied in detail. A spectrum of stationary, self-trapped (soliton) solutions is determined and tested for dynamic stability. Only those solutions for which the amide I energy is concentrated near a single molecule were found to be stable. Exciton modes were found to be unstable to decay into solitons.

I. INTRODUCTION

When crystalline acetanilide $(CH_3COHNC_6H_5)_x$ or ACN, is cooled below room temperature, a new amide I band (essentially CO stretching) appears in both Raman and infrared-absorption measurements with a red shift from the main peak of about 15 cm^{-1}.[1,2] It has recently been suggested that this new peak may be assigned to a self-trapping of amide I vibrational energy in a manner similar to that proposed by Davydov for α-helix in protein.[3] In the preceding paper[4] spectroscopic evidence is presented that precludes an assignment of the new band to: (i) a conventional amide I mode, (ii) crystal defect states, (iii) Fermi resonance, or (iv) frozen kinetics between two different subsystems. This conclusion is supported by detailed measurements of the crystal structure and specific heat as a function of temperature. Here, we assume that the self-trapping assignment is correct and discuss the theory in detail.

The self-trapping mechanism described here arises from an energetic interaction between amide I quanta and low-frequency phonons. Through this interaction, an amide I quantum causes shifts in the average positions of the ground states of the low-frequency vibrations. These shifts, in turn, act as a potential well to trap the amide I energy and prevent its dispersion by dipole-dipole interactions.

Self-trapping is not a new idea. It was introduced a half century ago in a note by Landau on the motion of an electron in a crystal lattice.[5] He suggested that an effect of the electron would be to polarize the crystal which, in turn, would lower its energy. Landau's suggestion was discussed in detail by Pekar[6] (who seems to have coined the term "polaron" for the localized electron plus lattice distortion), by Fröhlich,[7] and by Holstein.[8] Since 1970 the polaron has been studied by a number of authors.[9] In 1973 Davydov and Kislukha introduced the idea that molecular vibrational quanta can be self-trapped by acoustic phonons,[10] and Davydov suggested that this effect could be important in bioenergetics.[11]

What should these self-trapped states be called? Here, we use the term *soliton* to denote all self-trapped states (including the polaron) and many other localized, nonlinear states.[12]

The theory developed here follows closely the work of Davydov,[3] but we find that for reliable quantitative results it is necessary to account for the crystal structure and this introduces some novel aspects into the soliton theory. Our analytical and numerical methods are described in detail because they may be helpful in the investigation of similar effects in other crystals.

The basic quantum formulation of the problem is outlined in Sec. II and an exciton theory which accounts for the conventional ir and Raman bands is presented in Sec. III. In Sec. IV we determine the stationary (i.e., not moving) self-trapped states and discuss their dynamic stability. A dynamic calculation that suggests a tendency for exciton states to decay into solitons is presented in Sec. V. The appendices record details of our numerical codes and the crystal structure of ACN.

II. BASIC THEORY

The basic idea of Davydov's soliton theory is that amide I vibrational energy becomes self-trapped through interaction with low-frequency phonons.[3] Thus, the Hamiltonian operator is written

$$\hat{H}=\hat{H}_I+\hat{H}_l+\hat{H}_i\ . \tag{2.1}$$

Here, $\hat{H}_I$ is the energy operator for amide I vibrations including dipole-dipole interactions, thus

$$\hat{H}_I=\sum_{n,\alpha}\left[E_0\hat{B}^{\dagger}_{n\alpha}\hat{B}_{n\alpha}+\sum_{n',\alpha'}V(n,\alpha\,|\,n',\alpha')[\hat{B}^{\dagger}_{n\alpha}\hat{B}_{n'\alpha'}+\hat{B}^{\dagger}_{n'\alpha'}\hat{B}_{n\alpha}]\right], \tag{2.2}$$

where (see Fig. 1 and Appendix C) n is an index that counts unit cells in the b (or hydrogen-bonded) direction of the crystal and $\alpha(=1,2,3,\text{ or }4)$ specifies a particular molecule within one-half of the unit cell. In (2.2), E_0 is the energy of an amide I vibrational quantum excluding dipole-dipole interactions, and $\hat{B}^{\dagger}_{n\alpha}(\hat{B}_{n\alpha})$ is the corresponding boson creation (annihilation) operator.[13] (In interpreting Fig. 1, the reader may find it helpful to study the stereogram in Fig. 2.) The dipole-dipole—interaction energies are calculated from standard electromagnetic theory as

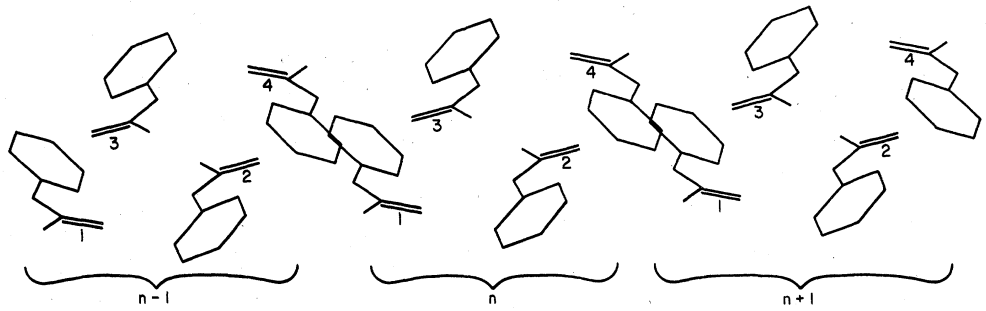

FIG. 1. Double hydrogen-bonded chain in ACN. In (2.2) the index n counts unit cells in the b direction. The index $\alpha(=1,2,3,4)$ specifies a particular molecule within the unit cell.

$$V(n,\alpha\,|\,n',\alpha')=\frac{D^2}{4\pi\kappa\epsilon_0 R^3}[\vec{e}_j\cdot\vec{e}_k-3(\vec{n}\cdot\vec{e}_j)(\vec{n}\cdot\vec{e}_k)]$$

$$=V_{jk}\ , \tag{2.3}$$

where $\vec{e}_j$ is a unit vector in the direction of the transition dipole moment of molecule (n,α) and $\vec{e}_k$ is the corresponding vector for molecule (n',α'). Also $\vec{n}$ is a unit vector in the direction joining the two dipoles, R is the distance between dipoles, and D $(=0.24$ D or 8.0×10^{-31} Cm[14]) is the transition dipole moment. From Ref. 15 this dipole is centered at a point 0.4 Å from O in the O—N direction, and from Refs. 16 and 17 it is oriented in the N—C=O plane about 20° from C=O toward the N—C direction. The intermolecular relative dielectric constant, κ, is assumed to be equal for all the interaction energies considered.

The low-frequency phonons are assumed to be a collection of R intramolecular and optical-mode vibrations which are described by coordinates $q_{n\alpha j}$ $(j=1,\ldots R)$. Neglecting contributions to optical-mode energy from interactions between unit cells, we write

$$\hat{H}_l=\sum_{n,\alpha}\sum_{j=1}^{R}\left[\frac{\omega_j^2}{2W_j}\hat{p}^2_{n\alpha j}+\tfrac{1}{2}W_j\hat{q}^2_{n\alpha j}\right]. \tag{2.4}$$

The interaction Hamiltonian takes into account that the site energy E_j depends on local distortion in the phonon field $q_{n\alpha j}$. Expanding E_j to first order in $q_{n\alpha j}$ yields $E_j\cong E_0+\chi_j q_{n\alpha j}$ where $\chi_j\equiv\partial E_j/\partial q_{n\alpha j}$. Thus the interaction Hamiltonian is

$$\hat{H}_i=\sum_{n,\alpha,j}\chi_j\hat{q}_{n\alpha j}\hat{B}^{\dagger}_{n\alpha}\hat{B}_{n\alpha}\ . \tag{2.5}$$

Following Davydov[3] we write the wave function for $\hat{H}$ as

$$|\psi\rangle=\sum_{n,\alpha}a_{n\alpha}(t)\exp(\hat{\sigma})\hat{B}^{\dagger}_{n\alpha}|0\rangle\ , \tag{2.6}$$

where

$$\hat{\sigma}\equiv-(i/\hbar)\sum_{n,\alpha,j}[q_{n\alpha j}(t)\hat{p}_{n\alpha j}-p_{n\alpha j}(t)\hat{q}_{n\alpha j}] \tag{2.7}$$

and

$$|0\rangle=|I,0\rangle\,|l,0\rangle\ , \tag{2.8}$$

where $|I,0\rangle$ is the ground state of $\hat{H}_I$ and $|l,0\rangle$ is the ground state of $\hat{H}_l$. From the normalization condition on $|\psi\rangle$,

$$\sum_{n,\alpha}|a_{n\alpha}|^2=1\ . \tag{2.9}$$

Also

$$\exp(\hat{\sigma}^{\dagger})\hat{q}_{n\alpha j}\exp(\hat{\sigma})=\hat{q}_{n\alpha j}+q_{n\alpha j}(t)\ , \tag{2.10a}$$

$$\exp(\hat{\sigma}^{\dagger})\hat{p}_{n\alpha j}\exp(\hat{\sigma})=\hat{p}_{n\alpha j}+p_{n\alpha j}(t)\ , \tag{2.10b}$$

thus

$$\langle\psi\,|\,\hat{q}_{n\alpha j}\,|\,\psi\rangle=q_{n\alpha j}(t)\ , \tag{2.11a}$$

$$\langle\psi\,|\,\hat{p}_{n\alpha j}\,|\,\psi\rangle=p_{n\alpha j}(t)\ . \tag{2.11b}$$

The equations of motion are obtained by applying variation methods to $\langle\psi\,|\,\hat{H}\,|\,\psi\rangle$:

$$i\hbar\dot{\vec{a}}_n=\mathrm{diag}[(E_0+E_s+\sum_j\chi_j q_{n1j}),\ldots]\vec{a}_n$$

$$+\frac{1}{\kappa}[\underline{M}\vec{a}_n+\underline{N}\vec{a}_{n+1}+\underline{N}^T\vec{a}_{n-1}]\ , \tag{2.12}$$

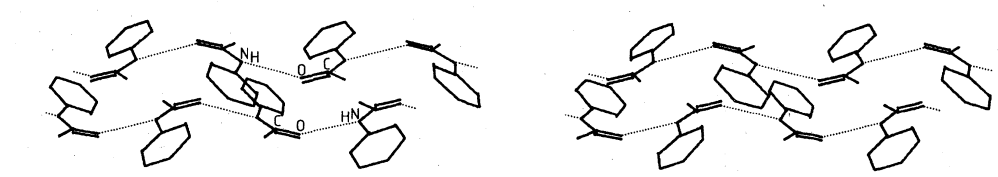

FIG. 2. Stereoscopic projection which may help the reader appreciate the structure of Fig. 1.

$$\frac{1}{\omega_j^2}\ddot{q}_{n\alpha j}+q_{n\alpha j}=-\frac{\chi_j}{W_j}\,|\,a_{n\alpha}\,|^2\,, \tag{2.13}$$

where

$$\vec{a}_n\equiv\mathrm{col}(a_{n1},a_{n2},a_{n3},a_{n4}) \tag{2.14}$$

and

$$E_s\equiv\sum_{n,\alpha,j}\left[\frac{W_j}{2\omega_j^2}\dot{q}^{\,2}_{n\alpha j}+\frac{W_j}{2}q^2_{n\alpha j}\right]. \tag{2.15}$$

The 4×4 matrix $\underline{M}$ represents the dipole-dipole interactions within one unit cell of the four molecules labeled n in Fig. 1. The 4×4 matrix $\underline{N}$ ($\underline{N}^T$) represents dipole-dipole interactions between the four molecules labeled n and those labeled $n+1$ ($n-1$) in Fig. 1. The matrix elements are calculated from (2.3); thus

$$\underline{M}=\begin{bmatrix}0 & -3.9604 & -3.5522 & 1.1287\\ -3.9604 & 0 & -0.1647 & -3.5522\\ -3.5522 & -0.1647 & 0 & -3.9604\\ 1.1287 & -3.5522 & -3.9604 & 0\end{bmatrix} \tag{2.16}$$

and

$$\underline{N}=\begin{bmatrix}-0.5490 & -0.1830 & 0.4394 & 0.1466\\ -3.9604 & -0.5490 & 0.6810 & 0.4394\\ 0.3445 & 0.0705 & -0.5490 & -0.1830\\ 1.7966 & 0.3445 & -3.9604 & -0.5490\end{bmatrix} \tag{2.17}$$

in units of cm^{-1}. Our primary purpose in this paper is to study (2.12) and (2.13).

III. EXCITON THEORY

As shown in Fig. 3, the ir-absorption spectrum of ACN in the amide I region exhibits four peaks which have been assigned as follows.[4]

Frequency (cm^{-1})	Assignment	Symmetry
1666	exciton (B_{2u})	y
1662	exciton (B_{3u})	x
1659	exciton (B_{1u})	z
1650	soliton	?

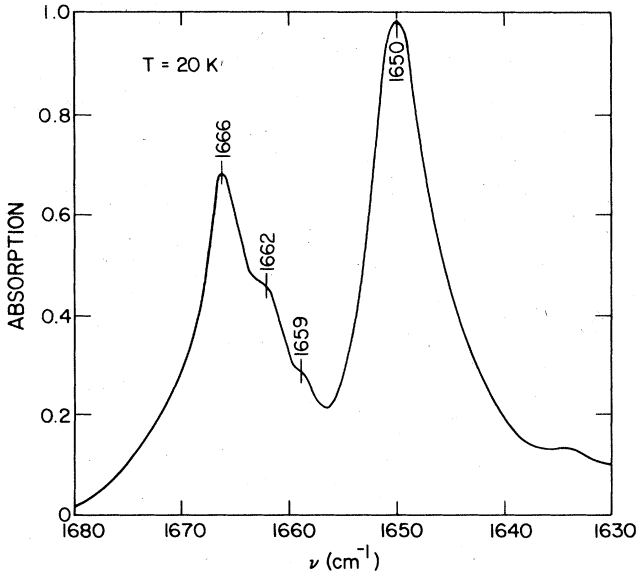

FIG. 3. Infrared-absorption spectrum of polycrystalline ACN at a resolution of 0.5 cm^{-1}. (Courtesy of E. Gratton; see Ref. 4 for experimental details.)

The B_{2u} mode has the property that y components of the amide I vibrations are in phase; thus it has the symmetry of a vector in the y direction. Modes B_{3u} and B_{1u} bear a similar relationship to vectors in the x and z directions, respectively.[18]

Since the exciton states are uniform over many unit cells of the crystal ($k=0$), the normalization condition (2.9) requires that $|\,a_{n\alpha}\,|^2\ll1$. This, in turn, implies that the source term $-(\chi_j/W_j)\,|\,a_{n\alpha}\,|^2$, on the right-hand side of (2.13) can be neglected. Thus (2.12) is decoupled from (2.13) and reduces to the linear Schrödinger equation

$$i\hbar\dot{\vec{a}}_n=E_0\vec{a}_n+\frac{1}{\kappa}(\underline{M}\vec{a}_n+\underline{N}\vec{a}_{n+1}+\underline{N}^T\vec{a}_{n-1})\,. \tag{3.1}$$

For $k=0$, $\vec{a}_n=\vec{a}_{n+1}=\vec{a}_{n-1}$. With the substitution

$$\bar{a}_n=\bar{\phi}\exp[-(i/\hbar)(E_0+E)]\,, \tag{3.2}$$

(3.1) takes the form

$$(\underline{M}+\underline{N}+\underline{N}^T-\underline{I}\kappa E)\vec{\phi}=0\,, \tag{3.3}$$

which has the following eigenvalues and eigenvectors:

$$\kappa E_1=-10.2115,\quad \bar{\phi}_1=\mathrm{col}(0.8922,1.0000,1.0000,0.8922)\,,$$
$$\kappa E_2=-8.4056,\quad \bar{\phi}_2=\mathrm{col}(1.0000,0.7939,-0.7939,-1.0000)\,,$$
$$\kappa E_3=2.5509,\quad \bar{\phi}_3=\mathrm{col}(-0.7939,1.0000,-1.0000,0.7939)\,,$$
$$\kappa E_4=11.6742,\quad \bar{\phi}_4=\mathrm{col}(1.0000,-0.8922,-0.8922,1.0000)\,.$$

From Fig. 1 it is seen that $\bar{\phi}_2$ has the B_{2u} symmetry of the 1666-cm^{1-} line. Also $\bar{\phi}_4$, which lies at an energy $1666+20.1/\kappa$, has the Raman-active (A_g) symmetry of the high-frequency lines in Fig. 13 of Ref. 4.

IV. SOLITON THEORY

We now consider the details of a soliton assignment for the 1650-cm^{-1} peak in the ir-absorption data of Fig. 3.

A. Nonlinear equations

We confine our attention to stationary solitons for which $\dot{q}_{n\alpha j}=0$. Thus from (2.13),

$$q_{n\alpha j}=-\frac{\chi_j}{W_j}|a_{n\alpha}|^2 \tag{4.1}$$

and (2.12) takes the form

$$i\hbar\dot{\vec{a}}_n=\mathrm{diag}[(E_0+E_s-\gamma|a_{n1}|^2),\ldots]\vec{a}_n + \frac{1}{\kappa}(\underline{M}\vec{a}_n+\underline{N}\vec{a}_{n+1}+\underline{N}^T\vec{a}_{n-1}), \tag{4.2}$$

where

$$E_s=\sum_{n,\alpha}\frac{\gamma}{2}|a_{n\alpha}|^4 \tag{4.3a}$$

and

$$\gamma\equiv\sum_j\frac{\chi_j^2}{W_j}. \tag{4.3b}$$

With the substitution

$$\vec{a}_n=\bar{\phi}_n\exp[-(i/\hbar)(E_0+E_s+E)], \tag{4.4}$$

(4.2) becomes

$$\underline{M}\bar{\phi}_n+\underline{N}\bar{\phi}_{n+1}+\underline{N}^T\bar{\phi}_{n-1}-\mathrm{diag}[\kappa(E+\gamma|\phi_{n1}|^2),\ldots]\bar{\phi}_n=0. \tag{4.5}$$

Since the 1666-cm^{-1} peak on Fig. 3 has energy E_0+E_2 and the 1650-cm^{-1} peak has energy E_0+E_s+E, the binding energy with respect to E_0+E_2 is

$$\Delta E=E_2-\frac{\gamma}{2}\sum_{n,\alpha}\phi_{n\alpha}^4-E. \tag{4.6}$$

Details of the solution procedure for (4.5) are presented in Appendix A, but the basic idea proceeds as follows. First we normalize $\bar{\phi}_n$ as

$$\bar{\phi}_n=(\kappa\gamma)^{-1/2}\bar{\psi}_n, \tag{4.7}$$

so (4.5) reduces to

$$\underline{M}\bar{\psi}_n+\underline{N}\bar{\psi}_{n+1}+\underline{N}^T\bar{\psi}_{n-1}-\mathrm{diag}[(\tilde{E}+|\psi_{n1}|^2),\ldots]\bar{\psi}_n=0, \tag{4.8}$$

where $\tilde{E}=\kappa E$. Next we find localized solutions of (4.8) which consist of the set $\{\bar{\psi}_n\}$ and its nonlinear eigenvalue $\tilde{E}$. From the normalization condition (2.9),

$$\kappa\gamma=\sum_{n,\alpha}\psi_{n\alpha}^2. \tag{4.9}$$

Finally, we determine $\kappa\Delta E$ from (4.6) as

$$\kappa\Delta E=\kappa E_2-\frac{1}{2\kappa\gamma}\sum_{n,\alpha}\psi_{n\alpha}^4-\kappa E. \tag{4.10}$$

As described in Appendix A, (4.8) is solved using a Newton iteration, working at fixed $\tilde{E}$. The success of this method depends on finding a good initial approximation $\bar{\psi}_n^{(0)}$ to the solution $\bar{\psi}_n$. Once a solution is obtained for a particular value of $\tilde{E}$, other solutions on the same branch for different values of $\tilde{E}$ can be found by continuation methods.[19] Other solutions on different branches can be generated by switching branches at a bifurcation point, or by an alternative choice of $\bar{\psi}_n^{(0)}$.

There are two regions where the choice of $\bar{\psi}_n^{(0)}$ is particularly simple. One is the linear regime, $\gamma=0$, where the $\tilde{E}$ and $\bar{\psi}_n$ are given (as in Sec. III) by the solution of a linear eigenvalue problem. The other region is for asymptotically large negative values of $\tilde{E}$, when the off-diagonal elements in (4.8) play a small role in the solution. In this case, we can effectively excite a fixed number of atomic sites by weighted δ functions which give a good approximation to the final solution. Once solutions on one of these two regions are known, the arclength continuation method enables solution branches to be followed into regions with intermediate values of $\tilde{E}$ and $\kappa\gamma$.

There are many solutions of (4.8). The linear problem has up to 100 independent eigenvalues and eigenvectors, and many more solutions are generated as the nonlinearity is increased. Some of these multiplicities correspond to degeneracies related to invariance under translation (in the approximation that boundary effects can be neglected), but there are other solutions of interest. In our numerical investigations, we have concentrated on solutions which are initially localized in one unit cell. The physical relevance and stability of these and other solutions are discussed in Sec. IV C: In the following section the discussion is purely concerned with numerical evidence for existence of solutions.

B. Stationary solutions

Since we are considering solutions localized within one unit cell, and there are four sites within our idealized unit cell, we can attempt to create solutions where one, two, three, or four sites in the cell are excited. For large $\gamma(\cong 40)$, solutions of all four types were found. Starting from these four solutions, we generated solution curves in these four cases. The results are summarized in Fig. 4, where any point on a curve denotes a distinct solution with the appropriate value of γ and ΔE. The solutions

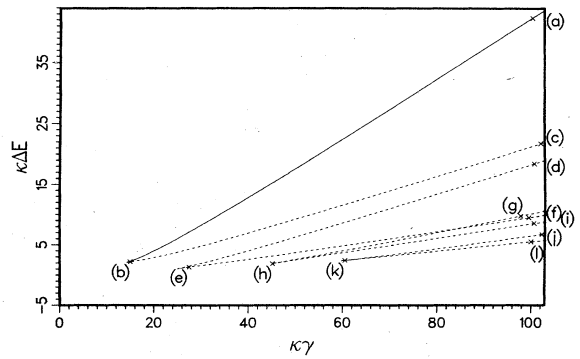

FIG. 4. Binding energy (with respect to the ir-active exciton) of several stationary solutions of (4.2). The relative dielectric constant (κ) is assumed to be the same for all dipole-dipole interactions. Only those solutions along the solid line were found to be dynamically stable.

corresponding to the points (a)—(l) are graphed in Figs. 5—8.

The simplest choice for $\vec{\psi}_n^{(0)}$ is to make $\vec{\psi}_n^{(0)}=\vec{0}$ at all sites, except for the atomic site (i,α), where we set $\psi_{i,\alpha}^{(0)}=c$. The choice of c will be discussed later. These initial conditions correspond physically to exciting a single molecule in the crystal. In all cases considered, we took a crystal of 25 unit cells (100 atomic sites). With $i=13$, $\alpha=1$ (site no. 1 in the central unit cell), $\tilde{E}=-40$, $c=6.3$, the Newton iteration converged to the solution shown in (a) of Fig. 5.

Symmetry considerations show an identical solution if $\alpha=1$ is replaced by $\alpha=4$, and this is confirmed by the numerical results. Very similar solutions are obtained if $\alpha=2$ or 3, but there is a slight energy shift (0.007) due to the fact that the two sites have slightly different crystal environments.

As γ decreases, this solution becomes less localized until at (b) (Fig. 5) it extends over several unit cells. The solution curve then turns around and develops into a curve with a solution having two adjacent sites excited, as shown in (c) (Fig.5).

Since we are interested in ir-active solutions, another choice of $\vec{\psi}_n^{(0)}$ is to take this initial solution to be nonzero on two sites in the unit cell, with opposite sign. Taking $\psi_{13,1}^{(0)}=-\psi_{13,4}^{(0)}=4.5$, $\tilde{E}=-20$ (other parameters unchanged) gives after the iteration has converged the solution shown in (d) of Fig. 6.

A similar solution is obtained if we take $\psi_{13,2}^{(0)}=-\psi_{13,3}^{(0)}=6$, but now there is an energy shift of 0.290. Following solution (d) (Fig. 6) as a function of γ gives the solution (e) (Fig. 6) for small γ, and another branch with a typical solution shown at (f) (Fig. 6).

Exciting three atomic sites in the unit cell gives the solution shown in (g) of Fig. 7. Other solutions shown on this curve are shown in (h) and (i) (Fig. 7).

The final possible choice is to excite each atom in the middle unit cell in an ir-active mode, by taking

$$\psi_{13,1}^{(0)}=\psi_{13,2}^{(0)}=-\psi_{13,3}^{(0)}=-\psi_{13,4}^{(0)}=3.2\ .$$

The resulting solution, with $\tilde{E}=-14$, is shown in (j) of Fig. 8. Other solutions on this curve are shown in (k) and (l) (Fig. 8).

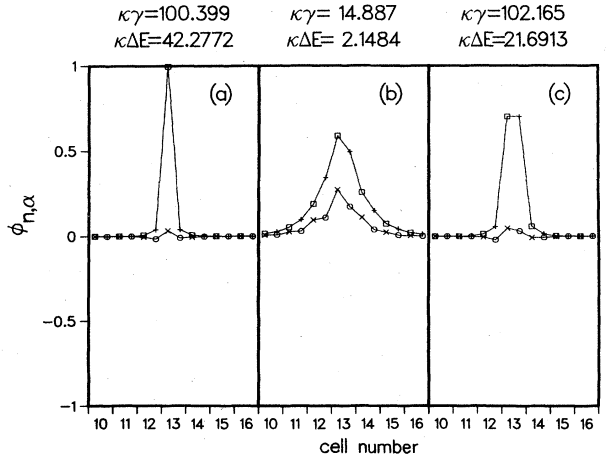

FIG. 5. Soliton structure at points (a), (b), and (c) of Fig. 4. The symbols □, +, × and ○ correspond to $\alpha=1$, 2, 3, and 4, respectively, in Fig. 1.

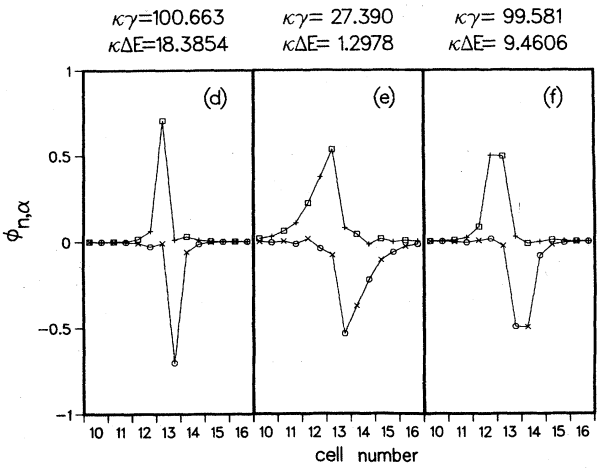

FIG. 6. Soliton structure at points (d), (e), and (f) of Fig. 4.

The linear forms of the curves shown in Fig. 4 away from the turning points can be explained by asymptotic arguments in a natural way. Assume the values of $\tilde{E}$ and $\vec{\psi}_n$ in (4.8) are such that the off-diagonal elements play no important part. Assume further that all the components of $\vec{\psi}_n$ are zero except for small number (m in all) components, which are all taken to be equal in value in order for $\tilde{E}$ to be constant over these sites. Then the equations which describe the nonzero elements take the form

$$(\tilde{E}+|\psi_{n\alpha}|^2)\psi_{n\alpha}=0\ , \tag{4.11}$$

so

$$\psi_{n\alpha}=(-\tilde{E})^{1/2}\ . \tag{4.12}$$

Hence,

$$\kappa\gamma=\sum_{n,\alpha}\psi^2=-m\tilde{E} \tag{4.13}$$

and for a fixed value of γ, the nonzero components of $\vec{\psi}_n$ are

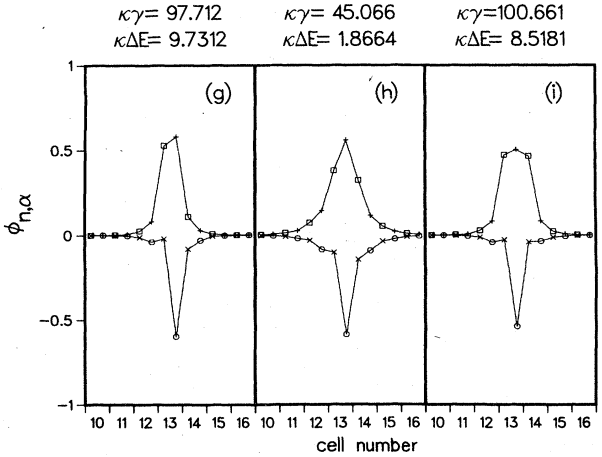

FIG. 7. Soliton structure at points (g), (h), and (i) of Fig. 4.

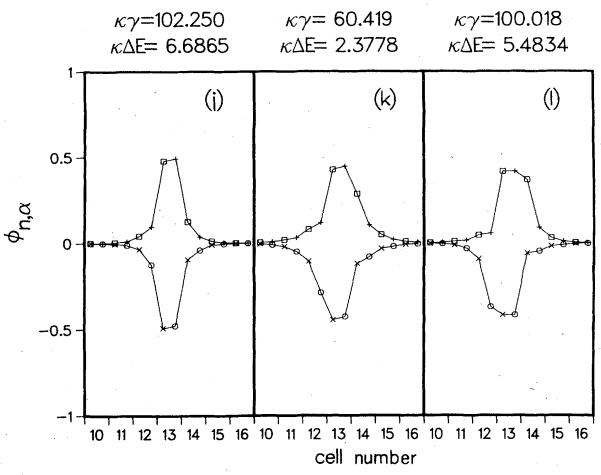

FIG. 8. Soliton structure at points (j), (k), and (l) of Fig. 4.

$$\psi_{n\alpha}=(\kappa\gamma/m)^{1/2} \tag{4.14}$$

which gives the value of the constant c discussed above. Putting these relations into (4.10) gives

$$\Delta E=E_2+\frac{\gamma}{2m}\ . \tag{4.15}$$

This result is in good agreement with the linear parts of the curves in Fig. 4. In particular, solution curves with only one site excited have slope $\frac{1}{2}$ on the graph [i.e., (b)—(a) (Fig. 4)], curves with two sites excited have slope $\frac{1}{4}$ [i.e., (b)—(c) and (d)—(e) (Fig. 4)], etc.

C. Dynamic stability

It is interesting to investigate the dynamic stability of the stationary soliton states found in the preceding subsection. In order to do so we have used these solutions as initial conditions for a numerical integration of the equations of motion for amide I energy with full dynamics retained. Details of the numerical code are given in Appendix B; here, we note that the equations of motion are

$$i\frac{da_j}{d\tau}=-|a_j|^2a_j+\frac{1}{\gamma}\sum_{k\ (\neq j)}V_{jk}a_k\ , \tag{4.16}$$

where j and k are running from 1 to N (number or peptide groups) and τ measures time in units of $\hbar/\gamma$. Equation (4.16) is slightly more general than (4.2), because it takes dipole-dipole interactions between all peptide groups into account—not only between nearest neighbors of the unit cell as in (4.2). The dipole-dipole interaction between peptide group j and k is given by the matrix element V_{jk}. The nearest-neighbor interaction equations (4.2) are therefore a subset of (4.16), and the additional dipole-interaction terms can be viewed as a small perturbation against which stability can be tested. On the other hand, we can solve (4.2) by adjusting the matrix elements V_{jk} to only include nearest-neighbor interactions.

We have tested the various stationary solutions found in Sec. IV B both with and without perturbations induced by the dipole interaction beyond nearest neighbor. Our findings can be summarized as follows. Most of the solutions are unstable to small perturbations and decay into the solution type shown in (a) of Fig. 5. A typical example is shown in Fig. 9—where the solution type shown in (f) of Fig. 6 is seen to decay into one which is focused on only one site [(a) of Fig. 5]—in addition small amplitude "radiation" is observed. A direct test of the stability of the solution focused only on one site [(a) of Fig. 5] showed that this state is stable for at least 1000 time units ($\sim$300 ps). The solution shown in (d) of Fig. 6 is the only one which is also stable for a similar amount of time—but when perturbed it decays very slowly into the solution of (a) in Fig. 5. It thus seems that only solutions where the energy is focused essentially on one peptide group in the unit cell [(a) of Fig. 5] are physically stable. This is consistent with the fact that the binding energy (ΔE) is largest for this type of solution (see Fig. 4).

D. Structure of the soliton

We now return to the fundamental motivation of this work: an assignment for the peak at 1650 cm^{-1} in Fig. 3. For the spectrum of stationary solutions of (4.2) that is displayed in Fig. 4, only those lying along the solid line were found to be dynamically stable. All solutions indicated by dashed lines are either unstable or have small basins of attraction, but the time constants for these instabilities vary widely. [For example, the decay shown in Fig. 9 takes place in about 20 ps, while decay of the solution shown in (d) of Fig. 6 requires about 200 ps.] Thus only the solid-line solutions are candidates for physical interpretation as the 1650-cm^{-1} peak in Fig. 3.

Our next problem is to determine an appropriate value for the relative dielectric constant (κ). In general, this is a difficult question because one is interested in the effective value of κ on the intermolecular distance scale which should lie somewhere between unity and the optical value of 2.62.[20] In Fig. 10 we display the structures of two stable soliton solutions that are chosen to have a binding energy (ΔE) of 15 cm^{-1}. The first solution is for $\kappa=2.62$ and the second for $\kappa=1$. Since the difference between these two solutions is small, our ignorance of the true effective value of κ is unimportant.

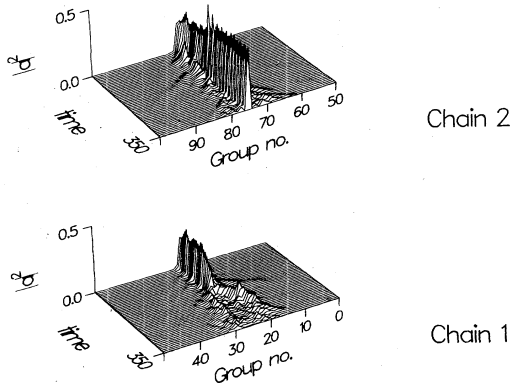

FIG. 9. Dynamic instability of the solution shown in (f) of Fig. 6. The parameters were $\kappa=2.51$ and $\gamma=30.42$. The time evolution is shown for approximately 60 ps.

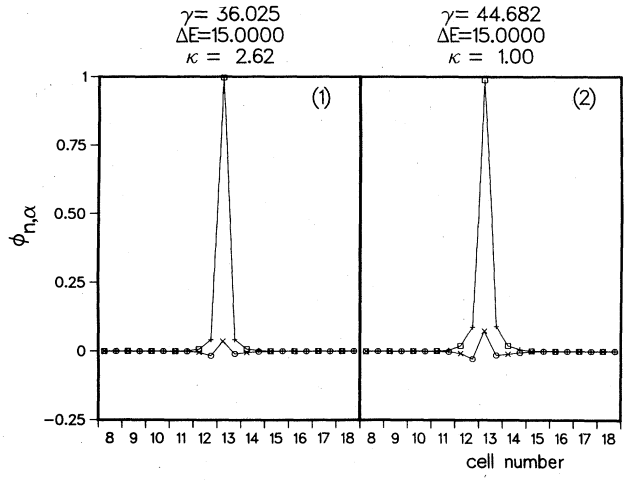

FIG. 10. Detailed structures of the dynamically stable solutions of (4.2) with $\Delta E=15$ cm^{-1} and $\kappa=1$ (vacuum) and 2.62 (optical).

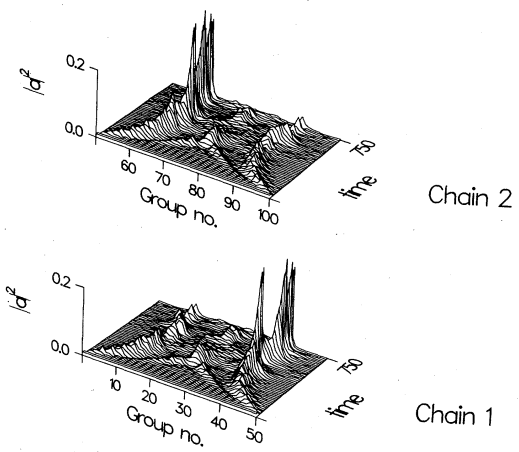

FIG. 11. Self-focusing or modulational instability of a uniformly distributed excitation (an exciton) representing one quantum of amide I vibrational energy. Two self-trapped states [resembling that of (a) in Fig. 5] are formed. The parameters were $\kappa=2.51$ and $\gamma=18.31$. The time evolution is shown for approximately 220 ps.

From Fig. 10 we see that the probability of finding a quantum of amide I vibrational energy is essentially localized on a single molecule. As discussed in Ref. 4, the magnitudes of the amide I transition dipole moments in the three crystal directions (a, b, and c) are 0.303, 0.934, and 0.191, respectively. Thus we expect the intensity of the 1650-cm^{-1} line to vary correspondingly as the incident wave polarization is changed.

V. DYNAMIC INSTABILITY OF EXCITONS

The relevance of the self-trapped states described in the preceding sections can also be appreciated by studying the dynamics of (4.16) with various initial conditions. We have found that initial conditions representing extended states self-organize into localized states when the full dynamics of (4.16) is taken into account. The nature of these localized states resembles the stable stationary states described in Sec. IV, but are in general more complex. They are not exact stationary states, but time dependent with oscillatory behavior.

In Fig. 11 we show an example of such a self-focusing phenomena. The initial condition, representing one quantum of amide I energy, is uniformly distributed over 25 unit cells and can thus also be viewed as a exciton with probability amplitude equal to 0.1. The energy is seen to focus into two solitonlike states which, although oscillating, resemble the stable stationary state [(a) of Fig. 5] found in Sec. IV. Where the energy is low on one chain it is found to be high on the other.

To understand the mechanism behind focusing into self-trapped states it is instructive to look at a simplified version of (4.16). If we only consider nearest-neighbor interaction along one chain of the ACN system and further replace the integer variable j with a continuous spatial variable xb (b being the lattice constant), (4.16) reduces to the nonlinear Schrödinger equation

$$ia_\tau+\Gamma a_{xx}+|a|^2a=0\ , \tag{5.1}$$

where $\Gamma=J/\gamma$ (J being the nearest-neighbor dipole-dipole–interaction matrix element). It is well known from plasma physics and fluid mechanics that this equation describes modulational (or Benjamin-Feir) instability. This means that a monochromatic wave train is unstable to modulations; the modulations will grow with time.

An argument due to Stuart and DiPrima[21] shows this phenomena in a simple manner. We will look for solutions of the form:

$$a(x,\tau)=[1+b(x,\tau)]a_0e^{i|a_0|^2\tau}\ . \tag{5.2}$$

This is a spatial modulation, $b(x,\tau)$, of the x-independent solution $a_0e^{i|a_0|^2\tau}$. Inserting (5.2) into (5.1) we obtain to first order in b,

$$ib_\tau+\Gamma b_{xx}+|a_0|^2(b^*+b)=0\ . \tag{5.3}$$

This equation is linear in b and we seek a solution of the form

$$b(x,\tau)=b_1e^{i(kx+\omega\tau)}+b_2e^{-i(kx+\omega^*\tau)}\ .$$

Inserting in (5.3) we find that the following relation must hold:

$$\omega^2=\Gamma k^2(\Gamma k^2-2|a_0|^2)\ . \tag{5.4}$$

When $Im(\omega)\neq0$ the waves described by $b(x,\tau)$ are unstable and will grow in time. This happens when $\Gamma k^2<2|a_0|^2$. The critical wavelength is thus

$$\lambda_{cr}=\frac{\pi}{a_0}(2\Gamma)^{1/2}\ . \tag{5.5}$$

For the solution shown in Fig. 11, we have $\gamma=18.31$, $J=1.58$, and $a_0=0.1$ which yields $\lambda_{cr}\cong13$. The wavelength found from Fig. 11 when the instability starts to grow ($t\cong300$) is $\lambda_{cr}\cong11$–12 in fair agreement with (5.5). At later times we enter a true nonlinear regime and the as-

sumptions leading to (5.3) break down. The qualitative aspects of the self-focusing mechanism are, however, still reasonably well described by (5.1) and we conclude that an exciton is unstable towards formation of self-trapped states.

VI. CONCLUSIONS

From the above discussion we draw the following conclusions.

(i) Although there are many stationary solutions that describe self-trapping in crystalline ACN, only those for which the amide I vibrational energy is localized on a single molecule were found to be dynamically stable.

(ii) The intensity of the 1650-cm^{-1} line in an ir-absorption measurement should stand in the ratios 0.303:0.934:0.191 as the incident beam polarization is oriented in the a, b, and c directions of the crystal.

(iii) Our dynamical studies indicate that an exciton mode is unstable to decay into a self-trapped solution. Whether this decay mechanism is sufficiently strong to compete with other modes of exciton decay is uncertain.

In addition to these specific conclusions, we feel that the analytical and numerical methods should be useful in the study of other materials that exhibit self-trapping of molecular vibrational energy, for example, para-chloroacetanilide.[4]

ACKNOWLEDGMENTS

It is a pleasure to thank E. Gratton for the infrared-absorption data plotted in Fig. 3 and L. MacNeil for the crystal-structure diagrams in Figs. 1, 2, and 12. One of the authors (J.C.E.) would like to acknowledge the Royal Society of London for partial financial support during the period that this work was being carried out, and the U.S.-United Kingdom Education Commission and the Carnegie Trust (Edinburgh) for further travel grants. The work was performed under the auspices of the U.S. Department of Energy with support from the Naval Air Systems Command.

APPENDIX A: NUMERICAL METHODS FOR THE STEADY-STATE EQUATIONS

The equation to be solved is (4.5):

$$\underline{M}\bar{\phi}_n+\underline{N}\bar{\phi}_{n+1}+\underline{N}^T\bar{\phi}_{n-1}-\mathrm{diag}[(\tilde{E}+\gamma|\phi_{n,1}|^2),\ldots,(\tilde{E}+\tilde{\gamma}|\phi_{n,4}|^2)]\bar{\phi}_n=0\ ,\quad n=1,2,3,\ldots,n_c\ . \tag{A1a}$$

Here, n_c is the number of unit cells in the crystal, $\underline{M}$ and $\underline{N}$ are 4×4 matrices, $\bar{\phi}_n$ is a 4-vector, and $\tilde{E}=\kappa E$ and $\tilde{\gamma}=\kappa\gamma$ are scalars. Since we are interested in localized solutions, we choose boundary conditions to force the solution close to zero at the ends of the crystal:

$$\bar{\phi}_0=\bar{\phi}_{n_c+1}=\vec{0}\ . \tag{A1b}$$

In all the numerical simulations, n_c was taken to be 25. The elements of matrices $\underline{N}$ and $\underline{M}$ are given in Sec. II. In (A1a), as elsewhere in this paper, the subscript T denotes matrix transposition.

If we introduce the $4n_c$ vector

$$\vec{\Phi}=[\bar{\phi}_1^T,\bar{\phi}_2^T,\ldots,\bar{\phi}_{n_c}^T]^T\ ,$$

the $4n_c\times4n_c$ block-tridiagonal matrix A, and the diagonal matrix $D(\Phi)$:

$$\underline{A}=\begin{bmatrix}\underline{M} & \underline{N} & \cdots & \cdots & \underline{0}\\ \underline{N}^T & \underline{M} & \underline{N} & \cdots & \vdots\\ \vdots & \underline{N}^T & \underline{M} & \underline{N} & \vdots\\ \vdots & \cdots & \cdots & \cdots & \vdots\\ \underline{0} & \cdots & \cdots & \underline{N}^T & \underline{M}\end{bmatrix}\ ,$$

$$\underline{D}=\begin{bmatrix}|\phi_{1,1}|^2 & \cdots & \cdots & 0\\ \vdots & |\phi_{1,1}|^2 & \vdots & \vdots\\ \vdots & \vdots & \vdots & \vdots\\ 0 & 0 & \cdots & |\phi_{n_c,4}|^2\end{bmatrix}\ ,$$

then (A1) can be written as

$$A\Phi-\tilde{E}\Phi-\tilde{\gamma}D(\Phi)\Phi=0\ . \tag{A2}$$

For fixed $\tilde{\gamma}$, Eq. (A2) is a nonlinear eigenvalue equation for the eigenvalue $\tilde{E}$ and the eigenvector Φ. Since A is symmetric, the solutions are all real, subject to an arbitrary constant phase change $\Phi\rightarrow\Phi e^{i\delta}$. In the case when $\tilde{\gamma}=0$ (see Sec. III), (A2) reduces to a *linear* eigenvalue problem for $(\tilde{E},\Phi)$ which can be solved by standard methods. Although our choice of boundary conditions (A1a) is slightly different from the periodic conditions for exciton solutions, the lowest linear eigenvalues of (A2) agree to a good approximation to those of (3.3).

If $\tilde{\gamma}$ is nonzero, it is possible to transform (A2) by the scaling $\Psi=\tilde{\gamma}^{1/2}\Phi$ to give

$$A\Psi-\tilde{E}\Psi-D(\Psi)\Psi=0\ . \tag{A3}$$

In this form we can *fix* $\tilde{E}$ and solve (A3) as a set of nonlinear simultaneous equations. Before considering this method of solution, we discuss briefly one method of solving the nonlinear eigenvalue problem (A2), the inverse power method.[22]

In this approach, the first step is to choose an initial guess $\tilde{E}^{(0)}$, $\Phi^{(0)}$ to the solution, with $\Phi^{(0)}$ normalized according to (2.9), i.e., $||\Phi^{(0)}||^2=1$. Then solve the *linear* set of equations

$$A\Phi^{(p+1)}-\tilde{E}^{(p)}\Phi^{(p+1)}-\tilde{\gamma}D(\Phi^{(p)})\Phi^{(p+1)}=0\ , \tag{A4}$$

where $p=0$, for the unknown vector $\Phi^{(p+1)}$. The next approximation to $\tilde{E}$ is then

$$\tilde{E}^{(p+1)}=\tilde{E}^{(p)}+(\Phi^{(p+1)},\Phi^{(p)})^{-1}\ , \tag{A5}$$

where the inner product (u,v) is the usual scalar or dot product $(u,v)=\Sigma u_i v_i$. The $(p+1)$th approximation $\Phi^{(p+1)}$ is then normalized to length unity before repeating the iteration beginning at (A4).

In practice, the inverse power method was found to converge quickly to some of the solutions found. However, in many cases the iteration converged slowly or not at all, unless the initial guess was very close to the desired solution. These convergence problems are due to the presence of close nearby eigenvalues and eigenvectors. In view of these problems, the use of this method cannot be recommended, except perhaps for the *linear* problem ($\tilde{\gamma}=0$), when the alternative methods described below break down.

When solving the nonlinear system (A3) for fixed $\tilde{E}$, there are several possible methods. One approach, used by Scott and MacNeil[23] for a simpler discrete nonlinear Schrödinger problem, is to solve (A3) by a shooting method. Since this method proved inappropriate for our particular problem, we shall not go into detail here. Due to the weak coupling between some of the atomic sites in the problem, a number of large but spurious eigenvalues appear which make an accurate calculation by this method extremely difficult. Another complication in this approach is the lack of reflection symmetry.

A more useful technique to solve (A3) for fixed $\tilde{E}$ is the standard Newton-Raphson iteration for a system of simultaneous nonlinear equations:

$$\Psi^{(p+1)}=\Psi^{(p)}-J^{(p)-1}F(\Psi^{(p)}),\quad p=0,1,\ldots, \tag{A6}$$

where

$$F(\Psi)=A\Psi-\tilde{E}\Psi-D(\Psi)\Psi$$

and $J^{(p)}$ is the Jacobian matrix

$$J_{i,j}^{(n)}=\frac{\partial F_i(\Psi^{(n)})}{\partial \Psi_j}\ .$$

Here the indices (i,j) range from (1,1) to $(4,n_c)$ over each atomic site. The matrix J has the same simple block-tridiagonal structure as F, and hence (A6) can easily be solved as a set of simultaneous equations for $\Psi^{(n+1)}-\Psi^{(n)}$:

$$J^{(n)}(\Psi^{(n+1)}-\Psi^{(n)})=F(\Psi^{(n)})\ . \tag{A7}$$

In practice it was found that the iteration converged very quickly except near singular points ($J^{(n)}$ singular).

Once we have a particular solution Ψ for a given value of $\tilde{E}$, solutions for nearby values of $\tilde{E}$ can be found using continuation methods.[19] In its simplest form this technique uses a Euler predictor as a starting point for the Newton iteration. Differentiating $F(\Psi,\tilde{E})=0$ with respect to $\tilde{E}$ gives

$$J(\Psi,\tilde{E})\frac{\partial\Psi}{\partial\tilde{E}}+\frac{\partial F}{\partial\tilde{E}}=0\ . \tag{A8}$$

Since $\partial F/\partial\tilde{E}=-\Psi$, this gives a simple (block-tridiagonal) set of equations for the vector $\partial\Psi/\partial\tilde{E}$. Then the first approximation to Ψ at $\tilde{E}+\Delta\tilde{E}$ is given by

$$\Psi^{(0)}(\tilde{E}+\Delta\tilde{E})=\Psi(\tilde{E})+\Delta\tilde{E}\frac{\partial\Psi}{\partial\tilde{E}}\ . \tag{A9}$$

This approximation to $\Psi(\tilde{E}+\Delta\tilde{E})$ is then used in the iteration (A6) in the usual way.

In regions where J is singular or near singular, the iteration breaks down and more sophisticated continuation techniques must be used. If we parametrize the solution curves by an arclength or pseudo arclength s, this singularity can be caused by a turning point at which $\partial\tilde{E}/\partial s=0$ (a simple limit point) or at bifurcation points.[19]

The continuation methods introduced by Kubicek, and Decker *et al.*[19] can enable limit points to be treated, and Decker *et al.* have also described methods for "shooting" from bifurcation points, which enables different branches originating from a bifurcation point to be followed. Full details are given in the references and will not be described here.

All the numerical codes were written in FORTRAN for a Cray-1 computer using the banded matrix routines in LINPACK. A more efficient variation would have been to use the block-tridiagonal equation-solver package due to Hindmarsh,[24] but these routines were not implemented at Los Alamos at the start of this study.

APPENDIX B: DYNAMICAL CODE

We have constructed a computer code GLOP (Ref. 25) to follow amide I energy in systems with arbitrary (random) geometry. The Hamiltonian for amide I energy in such a system with random dipole-dipole interactions is

$$\hat{H}_I=\sum_j E_0\hat{B}_j^{\dagger}\hat{B}_j+\sum_k\sum_{j\,(\neq k)}\frac{V_{jk}}{2}(\hat{B}_k^{\dagger}\hat{B}_j+\text{H.c.})\ , \tag{B1}$$

where $\hat{B}_j^{\dagger}$ and $\hat{B}_j$ are boson creation and annihilation operators for amide I excitation on the jth peptide group as described in the main text. The quantity V_{jk} is the dipole-dipole–interaction energy between groups j and k [see Eq. (2.3)]. A similar approach presented in Sec. II, yields the following equation of motion for amide I energy coupled to low-frequency phonons:

$$i\hbar\frac{d\tilde{a}_j}{dt}=(E_0+E_s)\tilde{a}_j-\gamma\,|\,\tilde{a}_j\,|^2\tilde{a}_j+\sum_{k\,(\neq j)}V_{jk}\tilde{a}_k\ . \tag{B2}$$

Here, the symbols have the same meaning as in Sec. II. Introducing $a_j(t)=\tilde{a}_j(t)e^{-i(E_0+E_s)t/\hbar}$, together with the scaled time variable $\tau=\gamma t/\hbar$, we obtain

$$i\frac{da_j}{d\tau}=-\,|\,a_j\,|^2a_j+\frac{1}{\gamma}\sum_{k\,(\neq j)}V_{jk}a_k\ . \tag{B3}$$

The code GLOP solves (B3) with any given initial condition after the dipole-dipole interactions have been calcu-

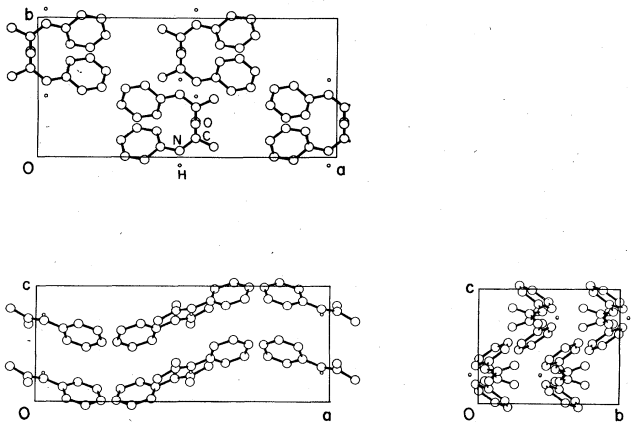

FIG. 12. Unit cell of ACN from atomic coordinates given in Ref. 20; $a=19.640$ Å, $b=9.483$ Å, and $c=7.979$ Å.

lated for the structure of interest, the atomic coordinates for this structure being the initial input. The equations of motion are integrated using a versatile leap-frog predictor-corrector method.[26] The accuracy of the integration is monitored at each time step via the conserved quantity: $\sum_j |a_j|^2=$constant. The code is fully vectorized for a Cray-1 computer and is very efficient.

APPENDIX C: CRYSTAL STRUCTURE OF ACN

From the atomic coordinates in Ref. 20, the structure of a unit cell of ACN is drawn in Fig. 12. The space group is D_{2h}^{15} (P_{bca}) and the unit cell or factor group is D_{2h}.[18] There are eight molecules in a unit cell and at the amide I frequency each of these has one degree of freedom. Thus there are three infrared-active modes (B_{1u}, B_{2u}, and B_{3u}), four Raman-active modes (A_g, B_{1g}, B_{2g}, and B_{3g}), and one inactive mode (A_u). All of these active modes are seen in ir-absorption and Raman experiments.[4]

At low frequencies (<200 cm^{-1}), ACN exhibits a complex spectrum of lattice vibrations which has been discussed in Refs. 4 and 27. Each molecule has six degrees of freedom (three of translation and three of rotation); thus there are a total of 48 low-frequency modes. Gerasimov has assigned the 24 Raman-active modes ($6A_g+6B_{1g}+6B_{2g}+6B_{3g}$) at 110 K.[27] In addition there are 18 ir-active modes ($6B_{1u}+6B_{2u}+6B_{3u}$) and six (A_u) modes corresponding to the acoustic modes of translation and rotation.

*Permanent and present address: Department of Mathematics, Heriot-Watt University, Riccarton, Edinburgh EH14 4AS, United Kingdom.

[1]G. Careri, *Cooperative Phenomena,* edited by H. Haken and M. Wagner (Springer, Berlin, 1973).

[2]G. Careri, U. Buontempo, F. Carta, E. Gratton, and A. C. Scott, Phys. Rev. Lett. **51**, 304 (1983).

[3]See A. S. Davydov, Phys. Scr. **20**, 387 (1979) for a summary of results and a bibliography.

[4]G. Careri, U. Buontempo, F. Galluzzi, A. C. Scott, E. Gratton, and E. Shyamsunder, preceding paper, Phys. Rev. B **30**, 4689 (1984).

[5]L. Landau, Phys. Z. Sowjetunion **3**, 664 (1933).

[6]S. Pekar, J. Phys. (Moscow) **10**, 341 (1946); **10**, 347 (1946).

[7]H. Fröhlich, H. Pelzer, and S. Zienau, Philos. Mag. **41**, 221 (1950); H. Fröhlich, Adv. Phys. **3**, 325 (1954).

[8]T. Holstein, Ann. Phys. (N.Y.) **8**, 325 (1959); **8**, 343 (1959).

[9]S. Fischer and S. A. Rice, J. Chem. Phys. **52**, 2089 (1970); H. Haken and P. Reineker, Z. Phys. **249**, 253 (1972); H. Sumi, J. Phys. Soc. Jpn. **32**, 616 (1972); H. Haken and G. Strobe, Z. Phys. **262**, 135 (1973); K. Tomioka *et al.*, J. Chem. Phys. **59**, 4157 (1973); W. Weidlich and W. Hendorfer, Z. Phys. **268**, 133 (1974); G. C. Morris and M. G. Sceats, Chem. Phys. **3**, 342 (1974); D. P. Craig and L. A. Dissado, *ibid.* **14**, 89 (1976); D. Yarkony and R. Silbey, J. Chem. Phys. **65**, 1042 (1976); D. P. Craig and L. A. Dissado, Chem. Phys. Lett. **44**, 419 (1976); D. P. Craig, L. A. Dissado, and S. H. Walmsley, *ibid.* **46**, 191 (1977); D. K. Campbell, A. R. Bishop, and K. Fesser, Phys. Rev. B **26**, 6862 (1982).

[10]A. S. Davydov and N. I. Kislukha, Phys. Status Solidi B **59**, 465 (1973).

[11]A. S. Davydov, J. Theor. Biol. **38**, 559 (1973).

[12]A. C. Scott, F. Y. F. Chu, and D. W. McLaughlin, Proc. IEEE **61**, 1443 (1973); R. K. Dodd, J. C. Eilbeck, J. D. Gibbon, and H. C. Morris, *Solitons and Nonlinear Wave Equations* (Academic, London, 1982).

[13]S. Takeno, Prog. Theor. Phys. **69**, 1798 (1983) proceeds by writing (2.2) as an Ising-like Hamiltonian which accounts for kinematic interactions. His results reduce to those of Davydov in the limit $J/E_0\rightarrow 0$.

[14]Yu. N. Chirgadze and N. A. Nevskaya, Dokl. Akad. Nauk SSSR **208**, 447 (1973).

[15]Yu. N. Chirgadze and N. A. Nevskaya, Biopolymers **15**, 607 (1976).

[16]N. B. Abbott and A. Elliott, Proc. R. Soc. London, Ser. A **234**, 247 (1956).

[17]M. Beer, G. B. B. M. Sutherland, K. N. Tanner, and D. L. Wood, Proc. R. Soc. London, Ser. A **249**, 147 (1959).

[18]D. L. Rousseau, R. P. Bauman, and S. P. S. Porto, J. Raman Spectrosc. **10**, 253 (1981).

[19]D. W. Decker and H. B. Keller, Commun. Pure Appl. Math. **34**, 149 (1981), and references therein; M. Kubicek, A. C. M. Trans. Math. Software **2**, 98 (1976).

[20]C. J. Brown and D. E. C. Corbridge, Acta Crystallogr. **7**, 711 (1954); C. J. Brown, *ibid.* **21**, 442 (1966).

[21]J. T. Stuart and R. C. DiPrima, Proc. R. Soc. London, Ser. A **362**, 27 (1978).

[22]S. D. Conte and C. de Boor, *Elementary Numerical Analysis* (McGraw-Hill, New York, 1980).

[23]A. C. Scott and L. MacNeil, Phys. Lett. **98A**, 87 (1983).

[24]A. C. Hindmarsh, Lawrence Livermore Laboratory Report No. UCID-30150, 1977 (unpublished).

[25]P. S. Lomdahl, Los Alamos Laboratory Report No. LA-UR-83-2252, 1983 (unpublished), and to appear in *Nonlinear Electrodynamics in Biological Systems,* edited by W. R. Adey and A. F. Lawrence (Plenum, New York, 1984).

[26]J. M. Hyman in *Nonlinear Problems: Present and Future* edited by A. R. Bishop, D. K. Campbell, and B. Nicolaenko (North-Holland, Amsterdam, 1982), p. 91.

[27]V. P. Gerasimov, Opt. Spektrosk. **43**, 705 (1977) [Opt. Spectrosc. (USSR) **43**, 417 (1977)].